Evidence for gravitational quadrupole moment variations in the companion of PSR J2051-0827

K. Lazaridis, J. P. W. Verbiest, T. M. Tauris, B. W. Stappers, M. Kramer, N. Wex, A. Jessner, Ismaël Cognard, G. Desvignes, G. H. Janssen, et al.

Monthly Notices
of the
ROYAL ASTRONOMICAL SOCIETY

Mon. Not. R. Astron. Soc. **414,** 3134–3144 (2011) doi:10.1111/j.1365-2966.2011.18610.x

Evidence for gravitational quadrupole moment variations in the companion of PSR J2051−0827

K. Lazaridis,[1] J. P. W. Verbiest,[1⋆] T. M. Tauris,[1,2] B. W. Stappers,[3,4] M. Kramer,[1,3] N. Wex,[1] A. Jessner,[1] I. Cognard,[5,6] G. Desvignes,[5] G. H. Janssen,[3] M. B. Purver,[3] G. Theureau,[5,6] C. G. Bassa[3] and R. Smits[3,4]

[1]*Max-Planck-Institut für Radioastronomie, Auf dem Hügel 69, 53121 Bonn, Germany*
[2]*Argelander-Institut für Astronomie, Universität Bonn, Auf dem Hügel 71, 53121 Bonn, Germany*
[3]*University of Manchester, Jodrell Bank Centre for Astrophysics, Alan Turing Building, Manchester M13 9PL*
[4]*Stichting ASTRON, Postbus 2, 7990 AA Dwingeloo, the Netherlands*
[5]*Laboratoire de Physique et Chimie de l'Environnement, CNRS, 3A Avenue de la Recherche Scientifique, 45071 Orléans Cedex 2, France*
[6]*Station de Radioastronomie de Nançay, Paris Observatory, CNRS/INSU, F45071 Nançay, France*

Accepted 2011 February 27. Received 2011 February 23; in original form 2011 January 3

ABSTRACT

We have conducted radio timing observations of the eclipsing millisecond binary pulsar PSR J2051−0827 with the European Pulsar Timing Array network of telescopes and the Parkes radio telescope, spanning over 13 yr. The increased data span allows significant measurements of the orbital eccentricity, $e = (6.2 \pm 1.3) \times 10^{-5}$, and composite proper motion, $\mu_t = 7.3 \pm 0.4$ mas yr^{-1}. Our timing observations have revealed secular variations of the projected semimajor axis of the pulsar orbit which are much more extreme than those previously published and of the orbital period of the system. Investigations of the physical mechanisms producing such variations confirm that the variations of the semimajor axis are most probably caused by classical spin–orbit coupling in the binary system, while the variations in orbital period are most likely caused by tidal dissipation leading to changes in the gravitational quadrupole moment of the companion.

Key words: binaries: eclipsing – stars: evolution – stars: fundamental parameters – pulsars: general – pulsars: individual: PSR J2051−0827.

1 INTRODUCTION

PSR J2051−0827 is the second eclipsing millisecond pulsar system discovered after the original black widow pulsar PSR B1957+20 (Fruchter, Stinebring & Taylor 1988). It was discovered (Stappers et al. 1996) as part of a Parkes all-sky survey of the southern sky for low-luminosity and millisecond pulsars. The pulsar has a spin period of 4.5 ms and inhabits a very compact circular orbit with a very low mass companion: $m_c < 0.1\,M_\odot$. The orbital period is $P_b = 2.38$ h and the pulsar and its companion are separated by just $1.0\,R_\odot$. Stappers et al. (1996, 2001a) investigated the eclipse characteristics of this system and found that their duration is ∼10 per cent of the orbital period at frequencies below 1 GHz. In addition, assuming a mean free electron density of 10^7 cm^{-3} in the eclipse region, they calculated a mass-loss rate of $\sim 10^{-14}\,M_\odot$ yr^{-1}, which is insufficient to evaporate the companion completely within a Hubble time.

Optical observations of the companion revealed that it is irradiated by the pulsar wind (Stappers, Bessell & Bailes 1996). Further observations and modelling of the variability of the light curve (Stappers et al. 1999; Stappers et al. 2001b) determined a binary inclination angle of $i \sim 40^\circ$, a backside temperature of $T \leq 3000$ K, a companion mass of $\sim 0.04\,M_\odot$ and a radius $\sim 0.064\,R_\odot$. An alternative model with a companion almost filling its Roche lobe ($\sim 0.12\,R_\odot$) was also considered and produced almost the same results, albeit with a significantly worse fit. For clarification purposes, a cartoon of the system is given in Fig. 1.

Doroshenko et al. (2001) presented the most precise timing analysis of PSR J2051−0827 using ∼6 yr of radio timing measurements with the Effelsberg 100-m radio telescope and the 76-m Lovell telescope at Jodrell Bank. Among the most important measurements is the variation of the projected semimajor axis, probably caused by Newtonian spin–orbit coupling (SOC) in this binary system. In addition, they measured significant orbital period variations and concluded that those were created by the same mechanism as in the B1957+20 system (Applegate & Shaham 1994; Arzoumanian, Fruchter & Taylor 1994): by tidal dissipation of a tidally powered, non-degenerate companion.

Because black widow (and other eclipsing) systems are susceptible to variations of their orbital parameters, monitoring over long lengths of time is crucial to understand these systems. Timing of black widow pulsars has been undertaken by Nice, Arzoumanian & Thorsett (2000) and Freire et al. (2003, 2005), but only very few of these systems have been monitored for a decade or longer. This is of particular interest given the large number of black widow

⋆E-mail: joris.verbiest@gmail.com

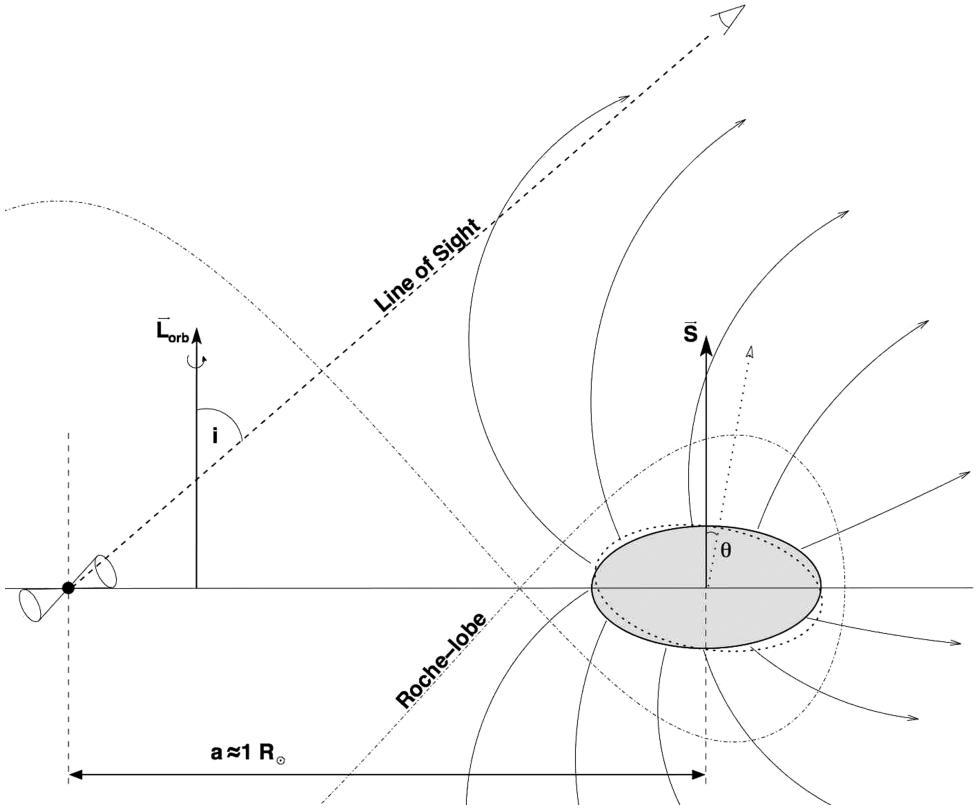

Figure 1. Illustration of the J2051−0827 system geometry. The pulsar and companion star are about $1\,R_{\odot}$ apart, the inclination angle of their orbit is approximately 40° and the pulsar wind pushes the companion's wind out, resulting in a bow shock-like denser region of charged particles, which causes the system to be eclipsed at given orbital phases and low observational frequencies. Changes in the oblateness of the tidally locked companion star, possibly in combination with alterations in the direction of the spin axis θ, trigger changes in the quadrupole moment that affect the timing of the pulsar. Note that this sketch is for illustrative purposes only and is not to scale.

pulsars recently found in unidentified *Fermi* sources (Keith et al. 2011; Ransom et al. 2011, and several discoveries that are soon to be published).

In this paper, we revisit PSR J2051−0827 with 13 yr of high-precision timing data and combined data sets from the Australia Telescope National Facility's Parkes 64-m radio telescope and the European Pulsar Timing Array (EPTA) telescopes, consisting of the 100-m Effelsberg radio telescope of the Max-Planck-Institute for Radioastronomy, Germany, the 76-m Lovell radio telescope at Jodrell Bank Observatory of the University of Manchester, UK, the 94-m-equivalent Westerbork Synthesis Radio Telescope (WSRT) of ASTRON, the Netherlands, and the 94-m-equivalent Nançay Decimetric Radio Telescope (NRT) of the Centre National de la Recherche Scientifique (CNRS), France. After describing the properties of our multitelescope data (Section 2), we present the updated measurements of the astrometric, spin and binary parameters for the system (Section 3). Specifically we show the measurement of the combined proper motion and of the orbital eccentricity of the PSR J2051−0827 system for the first time, and we measure the dispersion measure (DM) variations over time. Furthermore, we present the extreme variations in the orbital period and projected semimajor axis of the system, which are much larger than the ones published by Doroshenko et al. (2001). In Section 4, we rule out several possible contributions to the aforementioned variations and we discuss the physical mechanisms possibly responsible for those. Specifically, we show that gravitational quadrupole coupling (GQC) and classical SOC can be viable mechanisms for the orbital variations of the PSR J2051−0827 system, under certain assumptions. In light of the new orbital variation measurements, we discuss the possible scenarios for the nature of the companion and the prospects for observations of the system at higher energies. Finally, in Section 5, we briefly summarize our findings.

2 OBSERVATIONS AND DATA ANALYSIS

Description of the observing systems and the data acquisition procedure of the EPTA telescopes can be found in Lazaridis et al. (2009), while for Parkes this information is given in Stappers et al. (1998). A detailed description on combining pulse times of arrival (TOAs) from different telescopes can be found in Janssen et al. (2008) and Lazaridis et al. (2009); details specific to the data analysis used here are listed below.

In our timing of PSR J2051−0827, all TOAs with uncertainties greater than 20 μs were excluded as they do not impact the weighted fit. Furthermore, 573 TOAs that were taken at orbital phases between 0.2 and 0.35 were not used because the potential excess column density in the eclipsing region may cause additional modulation on the TOAs derived from these data (Stappers et al. 1998; Stappers et al. 2001a).

Timing was performed with the TEMPO2 software package (Hobbs, Edwards & Manchester 2006), using the DE405 Solar system ephemerides of the Jet Propulsion Laboratory (Standish 1998, 2004) and the ELL1 binary model (Lange et al. 2001). TEMPO2 minimizes the weighted sum of the squared residuals, producing a set of improved pulsar parameters and post-fit timing residuals. In order to propagate unmodelled noise into the uncertainties of the

Table 1. Properties of the individual telescope data sets.

Properties	Effelsberg	Jodrell Bank	Westerbork	Nançay	Parkes
Number of TOAs	490	139	46	2954	51
Time span (MJD)	50460–54791	49989–54853	54135–54845	53293–54888	49982–50343
Observed frequencies (MHz)	860, 1400, 2700	410, 606, 1400	330, 370, 840, 1380	1400	1400, 1700
Typical integration (min)	10	25	15	2	30

timing model parameters, the TOA uncertainties were multiplied by telescope-specific scaling factors to achieve a reduced χ^2 of unity. These scaling factors all fell between 1.4 and 3.5, where the largest factor was applied to the TOAs of the Effelsberg–Berkeley Pulsar Processor (EBPP). The large reduced χ^2 for the EBPP data is most likely caused by the fact that this instrument only records total power (no polarization information) and has no radio frequency interference (RFI) mitigation applied to it. Arbitrary phase offsets (also called 'jumps') were introduced between data obtained at different frequencies and/or taken with different telescopes to account for frequency-dependent pulse shape evolution and observatory-dependent differences in instrumental delays, cable lengths and geodetic position, amongst others. These jumps were included as free parameters in the least-squares fit performed by TEMPO2 and they absorb any non-changing dispersive effects in our data. Therefore, we were unable to evaluate the average DM and hence fixed the value obtained by Stappers et al. (1998) as a constant in our timing model. However, the data do contain some sensitivity to time-varying dispersive delays, which is fully discussed in Section 3.3.

In Table 1, the properties of the data from the different telescopes are presented. Combination of the TOAs from all the telescopes provides us with a 13-yr data set with no significant gaps. In order to obtain a coherent timing solution for this combined data set, higher order derivatives (up to the sixth order) of the orbital period and projected semimajor axis must be fitted, leading to high correlations between the modelled parameters. These variations in orbital period and size are discussed in detail in Sections 4.1 and 4.2. To avoid these correlations and because 85 per cent of our data (and all of our highest precision data) were taken after 2004, we derive the timing model, presented in Table 2, based solely on the last 4.5 yr of data, between MJDs 53293 and 54888 (as shown in Fig. 2). The remaining older data were exclusively used to investigate potential variations in interstellar dispersion (see Section 3.3) and to investigate possible causes for the variations in orbital period and projected semimajor axis (Section 3.5).

3 TIMING RESULTS

3.1 Proper motion

From the data shown in Fig. 2, we derived the first significant measurement of proper motion in both right ascension and declination. Using the NE2001 model for the Galactic distribution of free electrons (Cordes & Lazio 2002) and the pulsar's DM of 20.745 $\mathrm{cm^{-3}\,pc}$, a distance of $d \simeq 1040$ pc has been derived. Combining the latter with the composite proper motion, $\mu_t = 7.3 \pm 0.4\,\mathrm{mas\,yr^{-1}}$, the velocity of the system can be calculated as

$$v_t = \mu_t d = 36.1 \pm 7.5\,\mathrm{km\,s^{-1}}, \quad (1)$$

which is consistent with previous estimates (Stappers et al. 1998). The largest part of the error originates from the DM-derived distance where a 20 per cent uncertainty was assumed.

Table 2. Timing parameters for PSR J2051−0827 for the last epoch of observations (MJD range 53293–54888).

Parameters	EPTA
Right ascension, α (J2000)	$20^{\mathrm{h}}51^{\mathrm{m}}07\overset{\mathrm{s}}{.}51808(2)$
Declination, δ (J2000)	$-08^\circ27'37\overset{''}{.}7608(9)$
μ_α ($\mathrm{mas\,yr^{-1}}$)	6.6(2)
μ_δ ($\mathrm{mas\,yr^{-1}}$)	3.2(7)
ν (Hz)	221.796 283 737 706(1)
$\dot{\nu}$ ($\mathrm{s^{-2}}$)	$-6.2639(9) \times 10^{-16}$
P (ms)	4.508 641 818 284 89(2)
$\dot{P}$ ($\mathrm{s\,s^{-1}}$)	$1.2733(2) \times 10^{-20}$
Reference epoch (MJD)	54091
MJD range of global timing model	53293 – 54888
MJD range epoch 1	49989 – 51545
MJD range epoch 2	51384 – 52332
MJD range epoch 3	51967 – 53117
MJD range epoch 4	52790 – 54248
MJD range epoch 5	54156 – 54888
DM ($\mathrm{cm^{-3}\,pc}$)[a]	20.7458(2)
Orbital period, P_b (d)	0.099 110 248 46(2)
Projected semimajor axis, x (light-second)	0.045 0725(4)
η ($\equiv e \sin\omega$)	$5(1) \times 10^{-5}$
κ ($\equiv e \cos\omega$)	$4(1) \times 10^{-5}$
Eccentricity, e[a]	$6(1) \times 10^{-5}$
Longitude of the periastron, ω ($^\circ$)[a]	52(12)
T_ASC (MJD)	54091.0343503(1)
$\dot{P}_\mathrm{b}$, epoch 1 ($\mathrm{s\,s^{-1}}$)	$-1.33(6) \times 10^{-11}$
$\dot{P}_\mathrm{b}$, epoch 2 ($\mathrm{s\,s^{-1}}$)	$0.9(1) \times 10^{-11}$
$\dot{P}_\mathrm{b}$, epoch 3 ($\mathrm{s\,s^{-1}}$)	$1.8(3) \times 10^{-11}$
$\dot{P}_\mathrm{b}$, epoch 4 ($\mathrm{s\,s^{-1}}$)	$-1.81(3) \times 10^{-11}$
$\dot{P}_\mathrm{b}$, epoch 5 ($\mathrm{s\,s^{-1}}$)	$1.34(6) \times 10^{-11}$
$\dot{x}$, epoch 1 ($\mathrm{s\,s^{-1}}$)	$-1.7(4) \times 10^{-13}$
$\dot{x}$, epoch 2 ($\mathrm{s\,s^{-1}}$)	$-7.9(8) \times 10^{-13}$
$\dot{x}$, epoch 3 ($\mathrm{s\,s^{-1}}$)	$9(1) \times 10^{-13}$
$\dot{x}$, epoch 4 ($\mathrm{s\,s^{-1}}$)	$-0.8(2) \times 10^{-13}$
$\dot{x}$, epoch 5 ($\mathrm{s\,s^{-1}}$)	$0.2(2) \times 10^{-13}$
Solar system ephemeris model	DE405
Number of TOAs	3126
rms timing residual (μs)	12.2

[a]The eccentricity and the longitude of the periastron are calculated from the Laplace–Lagrange parameters, η and κ. The DM value and its uncertainty were taken from Stappers et al. (1998).

Figures in parentheses are the nominal 1σ TEMPO2 uncertainties in the least significant digits quoted.

These parameters were determined with TEMPO2, which uses the International Celestial Reference System and Barycentric Coordinate Time. Refer to Hobbs et al. (2006) for information on modifying this timing model for observing systems that use TEMPO format parameters.

3.2 Orbital eccentricity

PSR J2051−0827 is in a low-eccentricity binary. A precise eccentricity measurement has been challenging in the past but from our

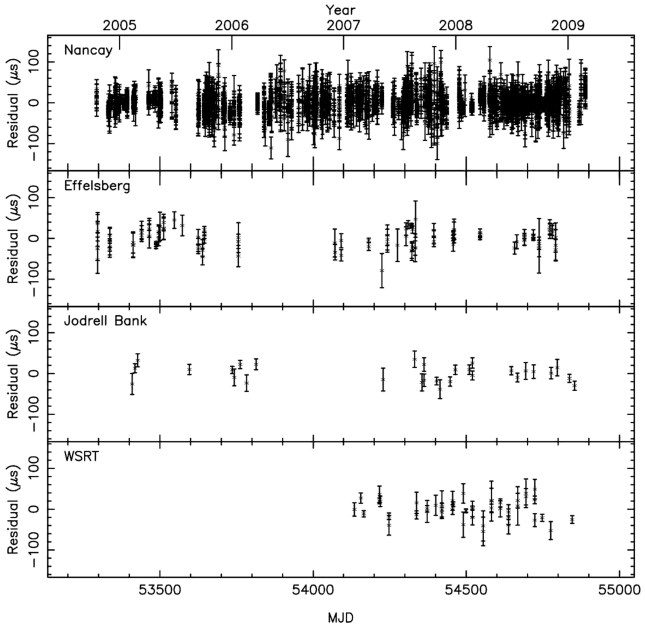

Figure 2. Post-fit timing residuals for the last 4.5 yr of data. Our timing solution is given in Table 2. The majority of the data are from the Nançay radio observatory, but data from Effelsberg, Jodrell Bank and Parkes were also used in the preceding 9 yr, which are not shown.

timing one has been made for the first time: $e = (6.2 \pm 1.3) \times 10^{-5}$. This eccentricity value is much larger than expected for such a tight binary system if plotted in an eccentricity versus orbital period diagram (as in Phinney 1992; Phinney & Kulkarni 1994). Although the model curves do not extend to very low orbital periods, this still constitutes evidence that the PSR J2051−0827 system at its present evolutionary stage experiences processes that do not allow for perfect circularization. These processes could very well be density fluctuations in a convective envelope of the donor star (see Section 4.1.1). Hence, the eccentricity of PSR J2051−0827 (6.2×10^{-5}) is much larger than the expected residual eccentricities ($\leq 10^{-8}$) for binary millisecond pulsars with a similar orbital period (Lanza & Rodonò 2001).

3.3 DM variations

As described in Section 1, low-frequency observations of this system show eclipses as the pulsar passes through periastron. This may imply increased dispersion as a function of orbital phase, which could corrupt measurements of binary parameters. To investigate this possibility, we took the high-quality, multifrequency data from the final 4.5 yr and measured the DM as a function of orbital phase while keeping the jumps between observing bands and observatories fixed. This did not result in significant trends at any orbital phase, including egress or ingress.[1] Since this experiment required a fit for DM over TOAs that were restricted to a small fraction of the binary phase, a simultaneous fit to standard orbital parameters was impossible. However, the wide frequency range available at any given orbital phase implies that even if orbital-phase-dependent DM variations did occur, their effect on the TOAs could only partially be absorbed by the orbital parameters, implying some residual DM

[1] This does not contradict the increased column density in the eclipse region but underlines the limited sensitivity of our data set to DM variations.

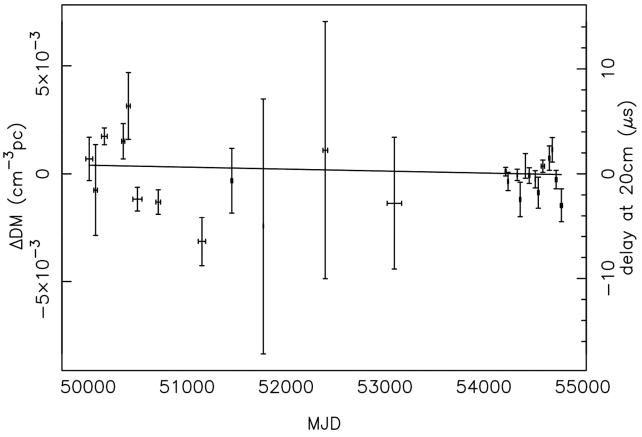

Figure 3. DM variations versus time, including the best-fitting linear trend.

variations would still be visible. Simultaneous fitting for DM and long-term effects (such as pulsar position and proper motion, spin, spin-down and orbital derivatives $\dot{P}_b$ and $\dot{x}$) over limited orbital-phase ranges did not affect the DM estimates or the other timing parameters, confirming that the long-period terms of the timing model are not affected by any potential orbital-phase-dependent variations in interstellar dispersion.

In addition to investigating the DM evolution as a function of orbital phase, the DM variations were determined across the entire data set. To this end, intervals with adequate multifrequency data were identified by hand and DM values were fitted in each interval, while jumps between telescopes and observing bands were kept fixed at the values determined from the entire data set. Clearly this cannot result in accurate measurements of DM, but it does allow variations to be determined precisely. The resulting measurements (shown in Fig. 3) demonstrate that no complex DM evolution is present in this data set, though a shallow DM decay is measured: $\mathrm{d(DM)/d}t = (-4.3 \pm 1.4) \times 10^{-4}\,\mathrm{cm^{-3}\,yr^{-1}\,pc}$. This measurement is barely significant at the 3σ level. Given the small number of high-quality DM estimates that contributed to it and the possible underestimation of the DM measurement uncertainties (e.g. variations in orbital parameters could have affected the offset between non-simultaneous observations), we did not include a time-dependent DM variation in our timing model.

3.4 Companion mass

Optical observations (Stappers et al. 2001b) yielded a best fit for the orbital inclination angle of about 40°. Depending on the unknown mass of the pulsar, this results in a companion mass in the range $m_c \simeq 0.04$–$0.06\,\mathrm{M_\odot}$ (see Fig. 4) given the constraints from the mass function

$$f = \frac{(m_c \sin i)^3}{(m_p + m_c)^2} = \frac{4\pi^2}{G}\,\frac{(a_p \sin i)^3}{P_b^2} = 1.0030 \times 10^{-5}\,\mathrm{M_\odot}, \qquad (2)$$

where the measured observable are the orbital period, P_b and the projected semimajor axis of the pulsar orbit, $a_p \sin i$. For the rest of this paper, we shall assume a companion star mass of $m_c = 0.05\,\mathrm{M_\odot}$ and consequently a pulsar mass of $m_p = 1.8\,\mathrm{M_\odot}$. The pulsar mass of PSR J2051−0827 is likely to be significantly larger than the typical neutron star mass ($1.35\,\mathrm{M_\odot}$) obtained from measurements in double neutron star binaries, given that this system has evolved through a long (∼Gyr) low-mass X-ray binary (LMXB) phase with sub-Eddington mass transfer (see e.g. Pfahl, Rappaport & Podsiadlowski 2002). Recent work on the mass determination of

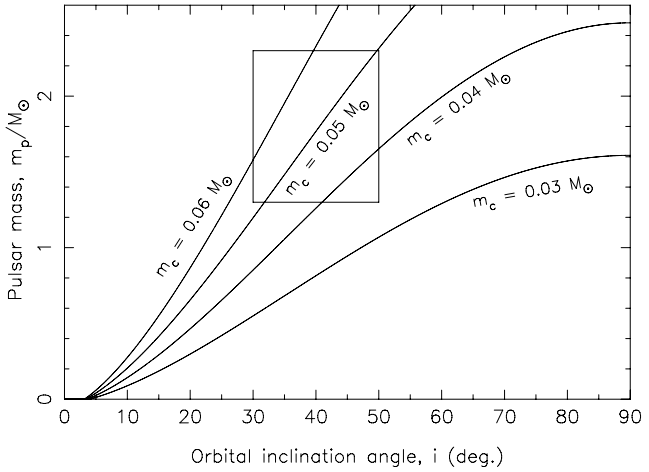

Figure 4. The masses of the stellar components in the J2051−0827 system as a function of orbital inclination angle. The box indicates the most likely parameter space in terms of the neutron star mass and constraints from radio eclipses and optical observations (see text).

the original black widow pulsar (PSR B1957+20) by van Kerkwijk, Breton & Kulkarni (2011) confirms that the pulsars in these systems can accrete significant amounts of matter. For a discussion of the effect of irradiation on the accretion efficiency in LMXBs, see Ritter (2008). The Roche lobe radius of the companion star in PSR J2051−0827 changes slightly with the estimated stellar masses and is found to be $R_{\rm L} = 0.15 \pm 0.01\,{\rm R}_\odot$. However, the size (radius) of the irradiated companion star is difficult to determine accurately, and in the discussion further on we shall assume two different values for the filling factor (the ratio of the volume-equivalent radius of the companion star to its Roche lobe) of 0.43 and 0.95 (Stappers et al. 2001b), corresponding to stellar radii of about 0.064 and 0.14 $\rm R_\odot$, respectively.

3.5 Orbital changes

In order to monitor their variations over time, values for $P_{\rm b}$ and x were derived for each year of data, where three months of overlap were kept between adjacent years. In doing so, all model parameters besides x, $P_{\rm b}$ and $T_{\rm ASC}$ were held fixed and the timing reference epoch was defined to be the centre of each year-long interval. The fractional changes of these measurements are shown in Fig. 5. Clearly, five different epochs can be identified, in which variations of both $P_{\rm b}$ and x can be described using only a linear trend, as shown in the figure.

4 DISCUSSION

4.1 Orbital period variations

$\dot{P}_{\rm b}$ is the observable rate of change of the orbital period and is caused by a variety of effects, both intrinsic to the system and caused by kinematic effects relative to the observer. The most important contributions are

$$\dot{P}_{\rm b} = \dot{P}_{\rm b}^{\rm GW} + \dot{P}_{\rm b}^{\rm D} + \dot{P}_{\rm b}^{in} + \dot{P}_{\rm b}^{\rm T} + \dot{P}_{\rm b}^{\rm Q}. \quad (3)$$

As a point of reference, the values for $\dot{P}_{\rm b}$ in the two most extreme epochs are $\dot{P}_{\rm b} = -1.81(3) \times 10^{-11}$ and $1.8(3) \times 10^{-11}$.

The first term, $\dot{P}_{\rm b}^{\rm GW}$, is the contribution due to gravitational wave emission. In general relativity, for circular orbits it is given by

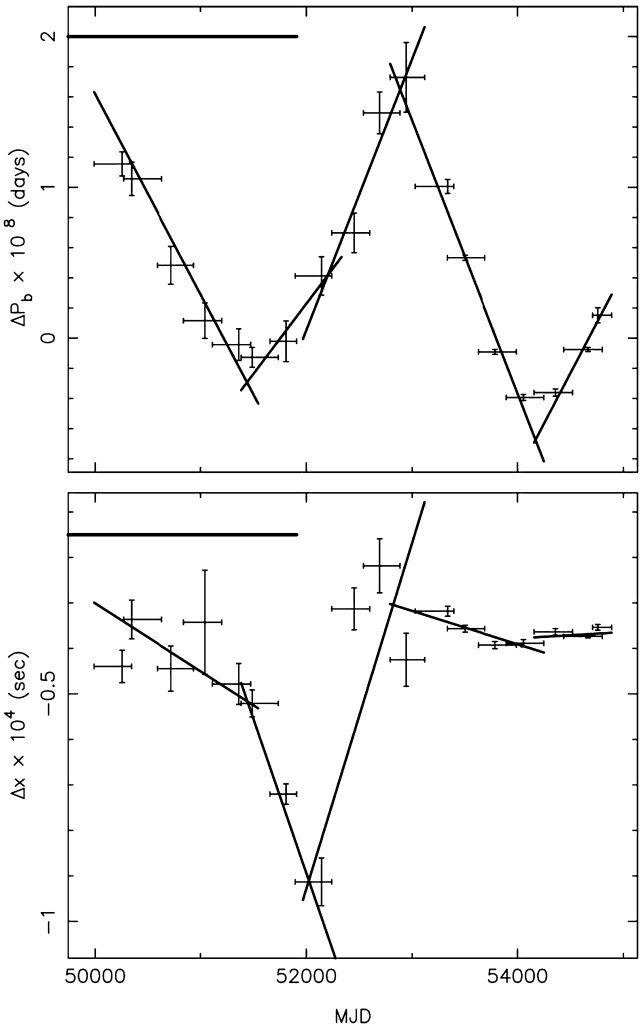

Figure 5. Changes of the orbital period (top panel) and projected semimajor axis (bottom panel) versus date. Each point corresponds to close to 1 yr of data, with typically three-month overlap between adjacent points, though the precise amount of overlap varies depending on the density of observations and the amplitude of the orbital variations. The horizontal bars indicate the intervals over which measurements were made, and the uncertainties of the measurements are shown by vertical error bars that are placed at the mean TOA of the data contained in the interval. Because of inhomogeneous sampling, the mean TOA is not necessarily at the middle of the interval. For each of the five epochs listed in Table 2, a trend line derived from the respective $\dot{P}_{\rm b}$ and $\dot{x}$ measurements given in Table 2 is shown. In most cases, these trend lines fit well through the measurement points, though deviations may be caused by rapid variations in orbital parameters, underestimation of measurement uncertainties, correlations between parameters and the fact that on many of the shorter measurement intervals only part of the timing model could be fitted for, incurring potential corruptions in correlated parameters. The thick horizontal bars on the top of the figure indicate the timing baseline of Doroshenko et al. (2001), which only really spans the first two of these epochs.

(Peters 1964)

$$\dot{P}_{\rm b}^{\rm GW} = -\frac{192\pi}{5}\left(\frac{2\pi}{P_{\rm b}}\frac{Gm_{\rm c}}{c^3}\right)^{5/3}\frac{q}{(q+1)^{1/3}}. \quad (4)$$

The mass ratio $q = 36$ has been calculated assuming a pulsar mass $m_{\rm p} = 1.8\,{\rm M}_\odot$ and a companion mass $m_{\rm c} = 0.05\,{\rm M}_\odot$ for an inclination angle of $i = 40^\circ$. For PSR J2051−0827, we find

$\dot{P}_{\rm b}^{\rm GW} \simeq -7.5 \times 10^{-14}$. This value is about three orders of magnitude less than the observed value of $\dot{P}_{\rm b}$.

The second term, $\dot{P}_{\rm b}^{\rm D}$, is the Doppler correction, which is the combined effect of the proper motion of the system (Shklovskii 1970) and a correction term for the Galactic acceleration. The contribution for the Galactic acceleration at the location of PSR J2051−0827, $\dot{P}_{\rm b}^{\rm Gal}$, is of the order of 1.1×10^{-15} (Lazaridis et al. 2009). Using numbers from Table 2, we also calculate the contribution due to the Shklovskii effect according to the following relation:

$$\dot{P}_{\rm b}^{\rm Shk} = \frac{(\mu_\alpha^2 + \mu_\delta^2)d}{c} P_{\rm b} \simeq 1.1 \times 10^{-15}. \quad (5)$$

By summing, we yield the Doppler correction

$$\dot{P}_{\rm b}^{\rm D} = \dot{P}_{\rm b}^{\rm Gal} + \dot{P}_{\rm b}^{\rm Shk} \simeq 2.2 \times 10^{-15}, \quad (6)$$

four orders of magnitude smaller than the measured value.

An acceleration of the binary system with respect to the Solar system barycentre (SSB) could also be caused by a third massive body orbiting the binary system. However, it would affect the orbital period derivative and the spin period derivative in the same way. Assuming that the spin period derivative is caused entirely by the acceleration, we can estimate the maximal effect this would have on $\dot{P}_{\rm b}$: $(\dot{P}_{\rm b}/P_{\rm b})^{\rm acc} = (\dot{P}/P) \simeq -3 \times 10^{-18}\,{\rm s}^{-1}$. This is seven orders of magnitude smaller than the measured value; thus there can be no massive third body orbiting the system.

The third term, $\dot{P}_{\rm b}^{\dot{m}}$, is the contribution from the mass-loss of the binary. If we consider a circular orbit, no mass-loss from the pulsar ($\dot{m}_{\rm p} = 0$) and a rate of mass-loss from the companion $\dot{m}_{\rm c} > 0$ (Jeans 1924), we obtain

$$\frac{\dot{P}_{\rm b}}{P_{\rm b}} = -2\frac{\dot{m}_{\rm c}}{M}, \quad (7)$$

and therefore

$$\dot{m}_{\rm c} = -\frac{M}{2}\frac{\dot{P}_{\rm b}}{P_{\rm b}} \simeq 6.2 \times 10^{-8}\,{\rm M}_\odot\,{\rm yr}^{-1}, \quad (8)$$

where M is the total mass of the system. This number is six orders of magnitude larger than expected (as calculated by Stappers et al. 1996) and hard to reconcile with the low electron densities measured in the eclipse region (Stappers et al. 1996). In addition, for the second of the epochs we would need mass injection to the companion in order to explain the orbital decay – an infeasible scenario for this system.

Tidal forces in tight synchronous binaries may also be responsible for interactions which would change the orbital period. This could be the case if, for example, a companion star suddenly contracts or expands and thereby changes its spin angular momentum. Tidal locking of the orbit would then result in exchange of spin and orbital angular momentum, e.g. Tauris & Savonije (2001). However, in PSR J2051−0827 we do not see reasons for any sudden major radial changes in the structure of the companion star – especially not changes that would not result in detection of X-ray bursts (Levine and Altamirano, private communication). Hence, we neglect the term $\dot{P}_{\rm b}^{\rm T}$.

Since all the above contributions are much smaller than the observed variation of the orbital period, we conclude that they must originate from the last term of equation (3), which represents variations of the gravitational quadrupole moment of the companion star.

4.1.1 The Applegate GQC model

The GQC mechanism (Applegate 1992; Applegate & Shaham 1994) has been applied successfully to the eclipsing binary system PSR B1957+20 (Applegate & Shaham 1994), explaining the orbital period variations seen by Arzoumanian et al. (1994). In addition, it was proposed by Doroshenko et al. (2001) as the main mechanism for producing the orbital period variations of PSR J2051−0827. However, as we will present below, the latter publication considered only a small part of these variations, which led to an underestimation in their calculations.

In the GQC model (Applegate & Shaham 1994), magnetic activity is driven by energy flows in convective layers of the irradiated companion. This, in combination with wind mass-loss, results in a torque on its spin, which holds it slightly out of synchronous rotation, causing tidal dissipation of energy and heating of the companion. The resultant time-dependent gravitational quadrupole moment (e.g. variations of the oblateness) causes modulation of the orbital period on a short, in principle dynamical, time-scale. An increase in the quadrupole moment causes the two stars to move closer together, and a decrease in the quadrupole moment results in a widening of the orbit – in Applegate model total orbital angular momentum is assumed to remain constant and the neutron star is treated as a point mass. The details of the hydrodynamic dynamo and its activity cycle remain unspecified for our purposes (also given the unknown nature of the companion star – see Section 4.4), and it is simply assumed that the variable quadrupole moment, ΔQ, is caused by cyclic spin-up and spin-down of the outer layers of the companion, which leads to orbital period changes equal to (Applegate & Shaham 1994)

$$\left(\frac{\Delta P_{\rm b}}{P_{\rm b}}\right)^{\rm Q} = -9\frac{\Delta Q}{m_{\rm c}a^2}, \quad (9)$$

where a is the separation and $m_{\rm c}$ is the companion mass. The transfer of angular momentum ΔJ to a thin shell of radius $R_{\rm c}$ and mass $M_{\rm s}$, rotating with angular velocity Ω in the gravitational field of a point mass $m_{\rm c}$, will cause the quadrupole moment of the shell to change by (Applegate & Shaham 1994)

$$\Delta Q = \frac{2}{9}\frac{M_{\rm s}R_{\rm c}^5}{Gm_{\rm c}}\,\Omega\,\Delta\Omega\,, \quad (10)$$

where G is the Newtonian gravitational constant and $\Delta\Omega$ is the change in the angular velocity of the shell. In order to produce orbital period changes $\Delta P_{\rm b}$, you need a variable angular velocity given by

$$\frac{M_{\rm s}}{m_{\rm c}}\frac{\Delta\Omega}{\Omega} = \frac{Gm_{\rm c}}{2R_{\rm c}^3}\left(\frac{a}{R_{\rm c}}\right)^2\left(\frac{P_{\rm b}}{2\pi}\right)^2\frac{\Delta P_{\rm b}}{P_{\rm b}} \quad (11)$$

(Applegate & Shaham 1994). This procedure produces a luminosity variation ΔL given by

$$\Delta L = \frac{\pi}{3}\frac{Gm_{\rm c}^2}{R_{\rm c}P_{\rm mod}}\left(\frac{a}{R_{\rm c}}\right)^2\frac{\Omega_{\rm dr}}{\Omega}\frac{\Delta P_{\rm b}}{P_{\rm b}}, \quad (12)$$

where $P_{\rm mod}$ is the period of the orbital period modulation and $\Omega_{\rm dr}$ is the angular velocity of the differential rotation (Applegate & Shaham 1994).

Applegate & Shaham (1994) assume in their model a mass $M_{\rm s} \simeq 0.1m_{\rm c}$ for the thin shell, an angular velocity $\Omega_{\rm dr} \simeq \Delta\Omega$ and luminosity variations at the $\Delta L/L \simeq 0.1$ level. From Fig. 5, we calculated for PSR J2051−0827 a total change in the orbital period of $\Delta P_{\rm b}/P_{\rm b} \simeq 2.2 \times 10^{-7}$ and a modulation period of $P_{\rm mod} \simeq 7.5$ yr. As mentioned above, these two values where underestimated and overestimated, respectively, in Doroshenko et al. (2001) because of their

significantly smaller data set. By assuming an inclination angle of $i = 40^\circ$ and a companion radius of $R_c \sim 0.064\,R_\odot$ (Stappers et al. 2001b) for a separation $a \simeq 7.1 \times 10^8$ m and a companion mass $m_c = 0.05\,M_\odot$, we derive a variation of the angular velocity of the companion of

$$\frac{\Delta\Omega}{\Omega} \sim 4 \times 10^{-2}. \quad (13)$$

This variation would produce a variable luminosity of $\Delta L \sim 1.4 \times 10^{33}\,\mathrm{erg\,s^{-1}}$, and according to the model the internal luminosity of the companion must be

$$L \sim 1.4 \times 10^{34}\,\mathrm{erg\,s^{-1}}. \quad (14)$$

From the optical observations of the companion (Stappers et al. 2001b), we can estimate a maximum effective temperature of $T_{\rm eff}^{\rm max} \simeq 3000\,\mathrm{K}$ which gives an internal luminosity of $L \sim 10^{30}\,\mathrm{erg\,s^{-1}}$. We therefore conclude that, under the assumptions listed above, the GQC model produces much larger orbital period variations than expected and cannot fit the PSR J2051−0827 system. If the companion was tidally powered, the internal luminosity derived from the optical observations would be much higher. One reason why GQC does not fit the observations may be the simplifications of the model itself, i.e. the consideration that all of the energy variations appear as luminosity variations without any loss (Applegate 1992). Although improvement of the model could possibly decrease ΔL by a factor of a few, the difference we calculate is significantly larger.

The previous calculations can change by a large factor if we consider the alternative model that Stappers et al. (2001b) presented for the companion star, where the latter almost fills its Roche lobe ($R_c = 0.14\,R_\odot$). Using the values for that model, we derive a variation of the angular velocity of the companion of

$$\frac{\Delta\Omega}{\Omega} \sim 7.1 \times 10^{-4} \quad (15)$$

and an internal luminosity of

$$L \sim 2 \times 10^{31}\,\mathrm{erg\,s^{-1}}. \quad (16)$$

This number is much closer to the newly calculated internal luminosity from the optical of $L \sim 6 \times 10^{30}\,\mathrm{erg\,s^{-1}}$. Thus, under specific assumptions, the GQC model can explain the orbital period variations of PSR J2051−0827.

4.2 Changes in the projected semimajor axis

The observed values of $\dot{x}$ can be the result of various effects (Lorimer & Kramer 2005):

$$\dot{x}_{\rm obs} = \dot{x}^{\rm GW} + \dot{x}^{\rm D} + \frac{{\rm d}\epsilon_{\rm A}}{{\rm d}t} + \dot{x}^{\rm PM} + \dot{x}^{\dot{m}} + \dot{x}^{\rm Q} + \dot{x}^{\rm SOC}. \quad (17)$$

For the most extreme epochs, we have $\dot{x} = -7.9(8) \times 10^{-13}$ and $9(1) \times 10^{-13}$.

The first term, $\dot{x}^{\rm GW}$, arises from orbital shrinkage due to gravitational-wave damping. Using Kepler's third law and equation (4),

$$\frac{\dot{x}^{\rm GW}}{x} = \frac{2}{3}\frac{\dot{P}_{\rm b}^{\rm GW}}{P_{\rm b}} \simeq -2.6 \times 10^{-19} \quad (18)$$

(Peters 1964). This contribution is much smaller than the current measurement.

The second term, $\dot{x}^{\rm D}$, is identical to the second term of equation (3). The contribution for the Galactic acceleration is of the order of 1.1×10^{-15} and the contribution of the Shklovskii effect $\dot{x}^{\rm Shk} = x(\mu_\alpha^2 + \mu_\delta^2)d/c \sim 6.0 \times 10^{-21}$. Both of these are very small compared to the observed value, so this term can be neglected.

The third term, ${\rm d}\epsilon_{\rm A}/{\rm d}t$, is the contribution of the varying aberration caused by geodetic precession of the pulsar spin axis and is typically of order $\Omega^{\rm geod} P/P_{\rm b} \approx 7.4 \times 10^{-17}$ (Damour & Taylor 1992). For a recycled pulsar, like PSR J2051−0827, the spin is expected to be close to parallel to the orbital angular momentum, which further suppresses this effect. Hence, the contribution is at least three orders of magnitude smaller than the observed value.

The fourth term, $\dot{x}^{\rm PM}$, represents a variation of x caused by a change of the orbital inclination, while the binary system is moving relatively to the SSB (Arzoumanian et al. 1996; Kopeikin 1996). This effect is quantified by the following equation:

$$\dot{x}^{\rm PM} = 1.54 \times 10^{-16}\, x\, \cot i\, (-\mu_\alpha \sin\Omega_{\rm asc} + \mu_\delta \cos\Omega_{\rm asc}), \quad (19)$$

where $\Omega_{\rm asc}$ is the position angle of the ascending node. The quantities x, μ_α and μ_δ are expressed in seconds and milliarcseconds per year, respectively. The maximal contribution of the proper motion is

$$\dot{x}^{\rm PM}_{\rm max} = 1.54 \times 10^{-16}\, x\, (\mu_\alpha^2 + \mu_\delta^2)^{1/2}\, \cot i. \quad (20)$$

For an inclination angle of $i = 40^\circ$, we get $\dot{x}^{\rm PM}_{\rm max} \simeq 6.0 \times 10^{-17}$. Thus, this term is also very small compared to the measured $\dot{x}$.

The fifth term, $\dot{x}^{\dot{m}}$, represents a change in the size of the orbit caused by mass-loss from the binary system. Using equation (7) and Kepler's third law, we calculate the rate of mass-loss from the companion to be seven to eight orders of magnitude larger than expected.

The sixth term, $\dot{x}^{\rm Q}$, is caused directly by the change in quadrupole moment as described in Section 4.1. Because orbital angular momentum is conserved in the Applegate model, a change in the orbital period is related to a change in the size of the orbit by

$$\frac{\Delta a}{a} = 2\frac{\Delta P_{\rm b}}{P_{\rm b}}. \quad (21)$$

It can be seen from Fig. 5 that this contribution falls short by four orders of magnitude to explain the observed changes in the projected semimajor axis x.

As all other contributions are much smaller than the observed variation of the projected semimajor axis, they must originate from the last term of equation (17): the classical SOC term.

4.2.1 The Applegate GQC model with SOC

Through SOC, the quadrupole of a rapidly rotating companion leads to apsidal motion and precession of the binary orbit. This in turn causes a variation of the longitude of periastron (which is impossible to measure in a system with such small eccentricity) and of the projected semimajor axis, according to

$$\dot{x}^{\rm SOC} = x\, n_{\rm b}\, \tilde{Q}\, \cot i\, \sin\theta\, \cos\theta\, \sin\Phi \quad (22)$$

(Smarr & Blandford 1976; Wex 1998), where $n_{\rm b} = 2\pi/P_{\rm b}$ is the orbital frequency, θ is the angle between the spin and orbital angular momentum and Φ is the longitude of the ascending node with respect to the invariable plane (plane perpendicular to the total angular momentum). The dimensionless quadrupole $\tilde{Q}$ is related to the quadrupole Q by

$$\tilde{Q} = \frac{3}{2} J_2 \left(\frac{R_c}{a}\right)^2, \quad J_2 = \frac{3Q}{m_c R_c^2}, \quad (23)$$

with J_2 the dimensionless measure of the quadrupole moment. Since no uniform change in x is detected, we can consider the companion

Table 3. Quadrupole moment variations for the five epochs, as derived from the P_b variations, alongside the x variations as observed.

Epoch	ΔQ (10^{45} g cm^2)	$n_b \Delta \tilde{Q}$ (10^{-11} s^{-1})	$\dot{x}/x$ (10^{-11} s^{-1})
1	11.2	7.7	−0.38
2	−4.6	−3.2	−1.8
3	−11.3	−7.7	2.0
4	14.3	9.8	−0.18
5	−5.3	−3.6	0.044

to consist of a long-term stable component with spin axis aligned to the orbital angular momentum axis (i.e. $\theta \approx 0$) and in addition to that, a part of the star (like e.g. an outer shell) that changes its quadrupole moment by $\Delta \tilde{Q}$ and has an effective and variable angle θ independent of the rest of the star. This part will then give rise to a variation $\dot{x}/x$ of order $n_b \Delta \tilde{Q}$.

In Section 4.1.1, we have described how changes in the gravitational quadrupole moment of the companion could cause the observed P_b variations. Even though these direct GQC effects are insufficient to explain the x variations (i.e. $\dot{x}^Q = 0$ as explained above), through the SOC mechanism they might have a more substantial effect.

Extending equation (9) to arbitrary θ and using equation (23), we have

$$\frac{\Delta P_b}{P_b} = -2\Delta \tilde{Q} \left(1 - \frac{3}{2}\sin^2\theta\right). \quad (24)$$

Combining this with the observed $\dot{P}_b$ values (Table 2) and assuming $\theta = 0$ for now, we get the maximum $\Delta \tilde{Q}$ values presented in Table 3. Comparison to the $\dot{x}/x$ values from Fig. 5, also listed in Table 3, shows that while the order of magnitude is roughly correct, the sign does neither correlate nor anticorrelate, which means that the orientation of the quadrupole moment changes (i.e. θ) must vary strongly from epoch to epoch, which may be unphysical.

In order to examine more closely if the orbital variations can be produced by GQC and SOC arising from the same ΔQ, we have plotted in Fig. 6 how $|\Delta \tilde{Q}|$ depends on θ, assuming $\Phi = 45^\circ$ and using $i = 40^\circ$. The curves are plotted for SOC, as derived from equation (22), and for GQC, as derived from equation (24). The intersection of the two lines clearly shows that for several values of θ, a $\Delta \tilde{Q}$ could explain both the orbital period and projected semimajor axis variations for PSR J2051−0827, though these θ values change significantly with epoch and we do not see how this easily fits with the physical mechanism behind the thin-shell model of Applegate (1992; see also our Section 4.1.1).

4.2.2 Spin precession of the companion star

In Section 4.2.1, we assumed a mostly stable companion star with an outer shell responsible for the changing quadrupole moment. An alternative explanation for the variations in P_b and x could be provided by limited quadrupole changes (as needed for the P_b variations, see Section 4.1.1) combined with an overall small tilt θ of the entire companion star with respect to the orbit. This tilt causes a precession of both the star and the orbit, and it allows the entire quadrupole moment of the star $\tilde{Q}$ to cause variations in x according to equation (22). We stress that in this scenario, there need not be a physical mechanism relating the spin precession (which causes the

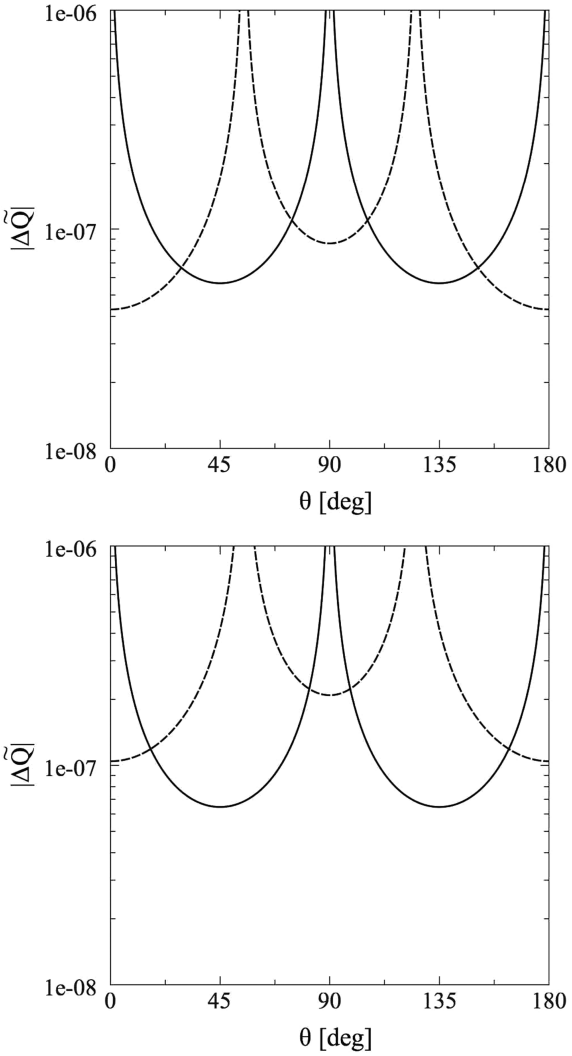

Figure 6. Quadrupole moment changes versus θ as produced by SOC (solid line) and GQC (dashed line) for epochs 2 (top panel) and 3 (bottom panel).

x variations) to the quadrupole moment changes (that induce the P_b changes).[2]

To evaluate this model, we estimate the quadrupole moment of the companion star assuming a non-degenerate structure[3] and following Lanza & Rodonò (1999):

$$Q = \frac{5}{6\xi}\,\frac{R^3\,[\mathcal{T} - (1-3\eta)\mathcal{M}]}{GM}, \quad (25)$$

where R and M are the radius and mass of the star, $\mathcal{T}$ is its rotational kinetic energy ($\mathcal{T} = I\Omega^2/2$), $\mathcal{M}$ is its total magnetic energy, η is the fraction of this magnetic energy in a field directed along the rotation axis and ξ is a dimensionless parameter depending on the density stratification and the spatial distribution of the perturbing forces in the convective layer of the star (it can be calculated from

[2] Note the changes in θ will have some contribution to the P_b changes as well. Based on equation (5) of Applegate (1992), we determined this effect and for all epochs save the third, this effect is at or well below the few per cent level of the P_b changes induced by ΔQ. In the third epoch, which requires the largest angle θ, it contributes 1 per cent of the observed P_b variations.

[3] Deviations of a semidegenerate nature should not be important in this case.

Table 4. Quadrupole moment changes (orientation and magnitude) that explain the changes in P_b and x for the five epochs.

Epoch	θ (°)	$\Delta Q/Q$
1	−0.14	+0.041
2	−0.64	−0.017
3	+0.73	−0.041
4	−0.06	+0.052
5	+0.02	−0.019

the gyration radius and the apsidal motion constant using stellar models). Here we shall use $\xi \simeq 5$. The rotational frequency of the outer layers of the star is taken to be that of the orbit (caused by synchronization) and in Applegate model $\mathcal{M} = 0$. Adopting a companion star radius $R = 0.064\,R_\odot$ yields

$$Q = 3.4 \times 10^{47}\,\mathrm{g\,cm^2}.$$

Consequently, the quadrupole moment Q of the star is one to two orders of magnitude larger than the variations required for the observed P_b changes. Using this value in equation (22) results in the angles θ required for the observed x variations. These values can in turn be used to correct the ΔQ values shown in Table 3 for the angular dependence, though this effect is all but negligible. The resulting changes required in the tilt and quadrupole moment of the companion star are collated in Table 4.

We conclude that with small changes in the orientation and magnitude of the quadrupole moment, we can explain all observed parameter changes. The change in the sign of $\dot{x}$ from one epoch to the other can be easily explained by a small oscillation of the symmetry axis of the quadrupole. Moreover, if we use an alternative scenario with a larger filling factor for the radius of the companion star, these numbers will get even smaller since Q will be larger. We do not, however, know of any physical mechanism that would cause the required tilt of the star or its rapid changes.

4.3 Alternative models for the gravitational quadrupole moment variations

The Applegate model is one of a number that have been applied to explain the cyclic modulation in the orbital period of magnetically active close binaries. In Applegate model, a rather large fraction of the stellar luminosity is required for its operation. Hence, one might be able to detect changes in the stellar luminosity in phase with the orbital period modulation. The model of Lanza & Rodonó (e.g. Lanza, Rodono & Rosner 1998; Lanza & Rodonò 1999) considers variations in the azimuthal B-field to explain the variations in oblateness. A change in the azimuthal field intensity can also produce a change in the quadrupole moment by changing the effective centrifugal acceleration. However, one should keep in mind that it remains to be established what kind of companion star we have in PSR J2051−0827.

4.4 The nature of the companion star

There seem to be three possibilities for the nature of the companion star:

(i) a white dwarf (WD);
(ii) a brown dwarf like star;
(iii) a semidegenerate helium star (He).

In the following, we briefly discuss each of these possibilities.

For a WD companion star of $M_c \geq 0.04\,M_\odot$, the mass–radius relation of a non-relativistic degenerate Fermi gas (e.g. Shapiro & Teukolsky 1983) yields an upper limit for the radius of $R_c \leq 0.025\,R_\odot$. This value is much less than what is estimated in optical since a combination of the minimum value for the filling factor of 0.43 and the Roche lobe size of $R_L = 0.15\,R_\odot$ yields a minimum optical radius of $R_c \geq 0.064\,R_\odot$. However, because of irradiation by the pulsar wind and tidal dissipation of energy in the WD envelope, it is likely that the WD is bloated in size. The effect of a thermally bloated WD in a close binary system has recently been detected in a transiting source by the *Kepler* satellite (Carter, Rappaport & Fabrycky 2011). In this case, the young (few hundred Myr) hot WD is bloated by a factor of 7 in size. The companion star in PSR J2051−0827 is believed to be much older; however, it is quite possible that an extended H-rich atmosphere may exist in this star from the effects mentioned above. On the other hand, the actual effect of the pulsar wind remains uncertain and may not be as efficient as expected previously. For example, equation (2) of Tavani (1992), for the irradiation of the companion as induced by the pulsar wind, yields a surface temperature of the companion of 6200 K. However, the observed temperature is ≤3000 K (Stappers et al. 2001b).

Brown dwarf models have been applied (Bildsten & Chakrabarty 2001) to explain the nature of the $\sim 0.05\,M_\odot$ donor star in the accreting millisecond pulsar system SAX J1808.4−3658. Brown dwarfs have a relation between mass and radius that is acceptable from observational constraints, also for PSR J2051−0827. However, the obtained mass–radius relation was based on brown dwarf models by Chabrier et al. (2000), calculated for isolated low-mass stars. We find it questionable if the present core remnant in PSR J2051−0827 can simply be described by the equivalent of a brown dwarf. The original zero-age main-sequence progenitor system of PSR J2051−0827 definitely did not consist of a B-star and a brown dwarf: the initial substellar mass of a brown dwarf is $<0.08\,M_\odot$ (the limit for H-ignition) and the progenitor of the neutron star had a mass $>10\,M_\odot$. Hence, the initial binary would have had a mass ratio of <1/100, which is not only disfavoured by formation, but also unlikely given that this binary should undergo a common envelope phase followed by survival of a supernova explosion and finally spin up the pulsar with so little mass. A more reasonable possibility is that PSR J2051−0827 (and many other eclipsing binary millisecond pulsars) is the outcome of a short orbital period, LMXB with unevolved main-sequence stars. Such systems have been studied in detail by e.g. Pylyser & Savonije (1988) and Ergma, Lundgren & Cordes (1997). The latter authors also discussed the final fate of a system like PSR J2051−0827: an ultracompact LMXB where the companion fills its Roche lobe (again), because of orbital angular momentum losses, and eventually may undergo tidal disruption leaving behind a single or planetary millisecond pulsar (e.g. a system like PSR B1257+12, Wolszczan & Frail 1992).

Finally, it should be noted that the companion star in PSR J2051−0827 could be closely related to the semidegenerate helium star companions in ultracompact AM CVn systems (e.g. Iben & Tutukov 1991; Nelemans et al. 2001). One example is the system SDSS J0926+3624 (Copperwheat et al. 2011) which has a similar companion mass of $0.035\,M_\odot$ ($P_b = 28$ min). Although the accreting compact object in AM CVn systems is a WD, a similar evolution is expected for systems with an accreting neutron star (Savonije, de Kool & van den Heuvel 1986). Also, in this case the expected mass–radius relations yield acceptable values for the radius in PSR J2051−0827 – especially if one accepts the possibility

that a pulsar wind and tidal dissipation could lead to a somewhat bloated radius.

4.5 High-energy emission prospects for PSR J2051−0827

The detection of X-rays from PSR J2051−0827 could yield vital information about its orbital evolution, the state of the companion star and interactions between the pulsar wind and the evaporated material of the companion star. However, no X-rays are detected from PSR J2051−0827 in the *RXTE* All Sky Survey (Levine, private communication). The *RXTE* All Sky Monitor (ASM) sensitivity in the 2–10 keV band is ∼30 mCrab, corresponding to an energy flux of $F_{\rm x} \simeq 7 \times 10^{-10}\,{\rm erg\,s^{-1}\,cm^{-2}}$. Given the distance to PSR J2051−0827 ($d \simeq 1.04$ kpc), we can estimate an upper limit to the mass accretion rate:

$$\dot{m} \leq \frac{4\pi d^2 F_{\rm x} R_{\rm p}}{G m_{\rm p}}. \quad (26)$$

Assuming a neutron star mass $m_{\rm p} = 1.8\,{\rm M}_\odot$ and radius $R_{\rm p} = 10^6$ cm, we obtain a conservative upper limit for the potential accretion rate $\dot{m} \lesssim 6.0 \times 10^{-12}\,{\rm M}_\odot\,{\rm yr}^{-1}$. Keeping in mind that the expected mass transfer rate for a Roche lobe filling ∼0.05 $\rm M_\odot$ companion star is expected to be much lower than this limit – and given the fact that we do observe a radio pulsar – it is not a surprise that PSR J2051−0827 is not detected in the *RXTE* ASM data. *Chandra* and/or *XMM* data would impose far more stringent constraints; or might even provide a detection.

One must bear in mind that the lack of detected X-rays does not exclude mass-loss from the companion star. It is possible that the pulsar wind (which is probably enhanced in the equatorial region towards the companion star) is able to prevent any accretion on to the neutron star. However, in this scenario it needs to be investigated thoroughly whether or not a shock front would lead to acceleration of protons and subsequent production of high-energy γ-rays (Harding & Gaisser 1990; Stappers et al. 2003).

Considering γ-ray emission from this system, with a distance of ≃1.04 kpc and a spin-down luminosity $\dot{E} = 4\pi^2 I \dot{P}/P^3 = 5.5 \times 10^{33}\,{\rm erg\,s^{-1}}$, this pulsar is a good candidate for detection with the Large Area Telescope of the *Fermi* satellite (Abdo et al. 2009). However, none of the *Fermi* sources in the first-year catalogue lies within a radius of 3° of PSR J2051−0827 (Abdo et al. 2010). It would therefore be interesting to see if PSR J2051−0827 is detected by *Fermi* with accumulated data.

5 SUMMARY

We have presented a timing update on PSR J2051−0827 and shown that the variations of the orbital period and projected semimajor axis of the binary system are far more extreme than described in earlier work. We have analysed all possible causes for these variations and found that a combination of GQC and SOC is the most likely origin of this behaviour, though accurate modelling efforts are still required. We furthermore discussed the nature of the companion star and conclude that a semidegenerate helium star is more likely than the WD alternative and, finally, we expect high-energy γ-rays to be visible in this system if a pulsar wind prevents accretion on to the neutron star – which in turn is expected based on the lack of X-rays.

ACKNOWLEDGMENTS

We are very grateful to all staff at the Effelsberg, Westerbork, Jodrell Bank and Nançay radio telescopes for their help with the observations used in this work. Part of this work is based on observations with the 100-m telescope of the Max-Planck-Institut für Radioastronomie (MPIfR) at Effelsberg. Access to the Lovell telescope is supported through an STFC rolling grant. The Nançay radio telescope is part of the Paris Observatory, associated with the Centre National de la Recherche Scientifique (CNRS) and partially supported by the Région Centre in France. The WSRT is operated by the Netherlands Foundation for Research in Astronomy (ASTRON) with support from the NWO. The Parkes radio telescope is part of the Australia Telescope National Facility which is funded by the Commonwealth of Australia for operation as a national facility managed by CSIRO. JPWV is supported by the European Union under Marie-Curie Intra-European Fellowship 236394. We want to thank Alan M. Levine (MIT) and Diego Altamirano (University of Amsterdam) for their help with investigating *RXTE* data, Lucas Guillemot (MPIfR) for discussions on *Fermi* results and Paulo Freire (MPIfR) for discussions on black widow and eclipsing systems. Finally, we thank the referee, Ingrid Stairs (UBC), for helpful and interesting comments.

REFERENCES

Abdo A. A. et al., 2009, Sci, 325, 848
Abdo A. A. et al., 2010, ApJS, 18, 405
Applegate J. H., 1992, ApJ, 385, 621
Applegate J. H., Shaham J., 1994, ApJ, 436, 312
Arzoumanian Z., Fruchter A. S., Taylor J. H., 1994, ApJ, 426, L85
Arzoumanian Z., Joshi K., Rasio F., Thorsett S. E., 1996, in Johnston S., Walker M. A., Bailes M., eds, ASP Conf. Ser. Vol. 105, Pulsars: Problems and Progress, IAU Colloq. 160. Astron. Soc. Pac., San Francisco, p. 525
Bildsten L., Chakrabarty D., 2001, ApJ, 557, 292
Carter J. A., Rappaport S., Fabrycky D., 2011, ApJ, 728, 139
Chabrier G., Baraffe I., Allard F., Hauschildt P., 2000, ApJ, 542, 464
Copperwheat C. M. et al., 2011, MNRAS, 410, 1113
Cordes J. M., Lazio T. J. W., 2002, preprint (astro-ph/0207156)
Damour T., Taylor J. H., 1992, Phys. Rev. D, 45, 1840
Doroshenko O., Löhmer O., Kramer M., Jessner A., Wielebinski R., Lyne A. G., Lange C., 2001, A&A, 379, 579
Ergma E., Lundgren S. C., Cordes J. M., 1997, ApJ, 475, L29
Freire P. C., Camilo F., Kramer M., Lorimer D. R., Lyne A. G., Manchester R. N., D'Amico N., 2003, MNRAS, 340, 1359
Freire P. C. C., Hessels J. W. T., Nice D. J., Ransom S. M., Lorimer D. R., Stairs I. H., 2005, ApJ, 621, 959
Fruchter A. S., Stinebring D. R., Taylor J. H., 1988, Nat, 333, 237
Harding A. K., Gaisser T. K., 1990, ApJ, 358, 561
Hobbs G. B., Edwards R. T., Manchester R. N., 2006, MNRAS, 369, 655
Iben I., Jr, Tutukov A. V., 1991, ApJ, 370, 615
Janssen G. H., Stappers B. W., Kramer M., Nice D. J., Jessner A., Cognard I., Purver M. B., 2008, A&A, 490, 753
Jeans J. H., 1924, MNRAS, 85, 2
Keith M. J. et al., 2011, preprint (astro-ph/1102.0648)
Kopeikin S. M., 1996, ApJ, 467, L93
Lange C., Camilo F., Wex N., Kramer M., Backer D., Lyne A., Doroshenko O., 2001, MNRAS, 326, 274
Lanza A. F., Rodonò M., 1999, A&A, 349, 887
Lanza A. F., Rodonò M., 2001, A&A, 376, 165
Lanza A. F., Rodono M., Rosner R., 1998, MNRAS, 296, 893
Lazaridis K. et al., 2009, MNRAS, 400, 805
Lorimer D. R., Kramer M., 2005, Handbook of Pulsar Astronomy. Cambridge Univ. Press, Cambridge
Nelemans G., Portegies Zwart S. F., Verbunt F., Yungelson L. R., 2001, A&A, 368, 939

Nice D. J., Arzoumanian Z., Thorsett S. E., 2000, in Kramer M., Wex N., Wielebinski R., eds, ASP Conf. Ser. Vol. 202, Pulsar Astronomy – 2000 and Beyond, IAU Colloq. 177. Astron. Soc. Pac., San Francisco, p. 67
Peters P. C., 1964, Phys. Rev., 136, 1224
Pfahl E., Rappaport S., Podsiadlowski P., 2002, ApJ, 573, 283
Phinney E. S., 1992, Philos. Trans. R. Soc. Lond. A, 341, 39
Phinney E. S., Kulkarni S. R., 1994, ARA&A, 32, 591
Pylyser E., Savonije G. J., 1988, A&A, 191, 57
Ransom S. M. et al., 2011, ApJ, 727, L16
Ritter H., 2008, New Astron. Rev., 51, 869
Savonije G. J., de Kool M., van den Heuvel E. P. J., 1986, A&A, 155, 51
Shapiro S. L., Teukolsky S. A., 1983, Black Holes, White Dwarfs and Neutron Stars. The Physics of Compact Objects. Wiley, New York
Shklovskii I. S., 1970, SvA, 13, 562
Smarr L. L., Blandford R., 1976, ApJ, 207, 574
Standish E. M., 1998, JPL Planetary and Lunar Ephemerides, DE405/LE405, Memo IOM 312.F-98-048. JPL, Pasadena
Standish E. M., 2004, A&A, 417, 1165
Stappers B. W. et al., 1996, ApJ, 465, L119
Stappers B. W., Bessell M. S., Bailes M., 1996, ApJ, 473, L119
Stappers B. W., Bailes M., Manchester R. N., Sandhu J. S., Toscano M., 1998, ApJ, 499, L183
Stappers B. W., van Kerkwijk M. H., Lane B., Kulkarni S. R., 1999, ApJ, 510, L45
Stappers B. W., Bailes M., Lyne A. G., Camilo F., Manchester R. N., Sandhu J. S., Toscano M., Bell J. F., 2001a, MNRAS, 321, 576
Stappers B. W., van Kerkwijk M. H., Bell J. F., Kulkarni S. R., 2001b, ApJ, 548, L183
Stappers B. W., Gaensler B. M., Kaspi V. M., van der Klis M., Lewin W. H. G., 2003, Sci, 299, 1372
Tauris T. M., Savonije G. J., 2001, in Kouveliotou C., Ventura J., van den Heuvel E., eds, Proc. NATO ASI Vol. 567. Ser C. The Neutron Star – Black Hole Connection Spin-Orbit Coupling in X-ray Binaries. Kluwer, Dordrecht, p. 337
Tavani M., 1992, in van den Heuvel E. P. J., Rappaport S. A., eds, X-ray Binaries and Recycled Pulsars. Kluwer, Dordrecht, p. 387
van Kerkwijk M. H., Breton R. P., Kulkarni S. R., 2011, ApJ, 728, 95
Wex N., 1998, MNRAS, 298, 67
Wolszczan A., Frail D. A., 1992, Nat, 355, 145

This paper has been typeset from a TEX/LATEX file prepared by the author.